In vivo FRET–FLIM reveals cell-type-specific protein interactions in *Arabidopsis* roots

Yuchen Long[1,2]†, Yvonne stahl[3], stefanie Weidtkamp-Peters[4], Marten Postma[5], Wenkun Zhou[1], Joachim goedhart[5], María-Isabel sánchez-Pérez[6], theodorus W. J. gadella Jr[5], Rüdiger simon[3], Ben scheres[1,2] & Ikram Blilou[1,2]

During multicellular development, specification of distinct cell fates is often regulated by the same transcription factors operating differently in distinct *cis*-regulatory modules[1–3], either through different protein complexes, conformational modification of protein complexes, or combinations of both. Direct visualization of different transcription factor complex states guiding specific gene expression programs has been challenging. Here we use *in vivo* FRET–FLIM (Förster resonance energy transfer measured by fluorescence lifetime microscopy) to reveal spatial partitioning of protein interactions in relation to specification of cell fate. We show that, in *Arabidopsis* roots, three fully functional fluorescently tagged cell fate regulators establish cell-type-specific interactions at endogenous expression levels and can form higher order complexes. We reveal that cell-type-specific *in vivo* FRET–FLIM distributions reflect conformational changes of these complexes to differentially regulate target genes and specify distinct cell fates.

In *Arabidopsis thaliana* roots, three co-expressed and interacting transcription factors, SHORT-ROOT (SHR), SCARECROW (SCR) and JACKDAW (JKD), activate genes in the cell layer surrounding the vasculature, referred to as the U-shaped domain (Fig. 1a, Extended Data Fig. 1) to specify three cell types: (1) the stem-cell-organizing quiescent centre (QC); (2) the cortex/endodermis initial (CEI), and (3) the endodermis[4–7]. Mobile SHR protein enters the U-shaped domain from the vasculature and induces *SCR* transcription to promote formative divisions that separate cortex and endodermis by activating *CYCLIN D6;1* (*CYCD6;1*) in the CEI[8–10]. SHR movement and specification of cell fate rely on protein–protein interactions with SCR and JKD[5]. To determine the distribution of protein–protein interactions in relevant contexts at cellular resolution, we optimized *in vivo* FRET–FLIM at physiological conditions in living *Arabidopsis* roots. We implemented time- and frequency-domain FLIM[11,12] to address whether SHR, SCR and JKD form spatially distinct protein–protein interaction patterns.

FRET describes energy transfer from fluorescently tagged 'donor' molecules to nearby 'acceptor' molecules (<10 nm, indicating protein–protein interaction), which causes a donor fluorescence lifetime decrease that is quantifiable by FLIM[13] (Fig. 1b). We established FRET between SHR, SCR, JKD and the JKD homologue NUTCRACKER (NUC) by optimizing fluorophore tag orientations in *Arabidopsis* mesophyll protoplasts (Fig. 1c, Extended Data Fig. 1d, e). We confirmed protein functionality under endogenous promoters by complementing respective mutant phenotypes (Extended Data Figs 2, 3). Endogenous JKD and NUC fusions were weak for FRET–FLIM measurements (Extended Data Fig. 4), therefore we moderately enhanced protein levels using *SCR* promoter (*pSCR*)-driven RFP-fused acceptors to ensure donor saturation (donor ≤ acceptor), while

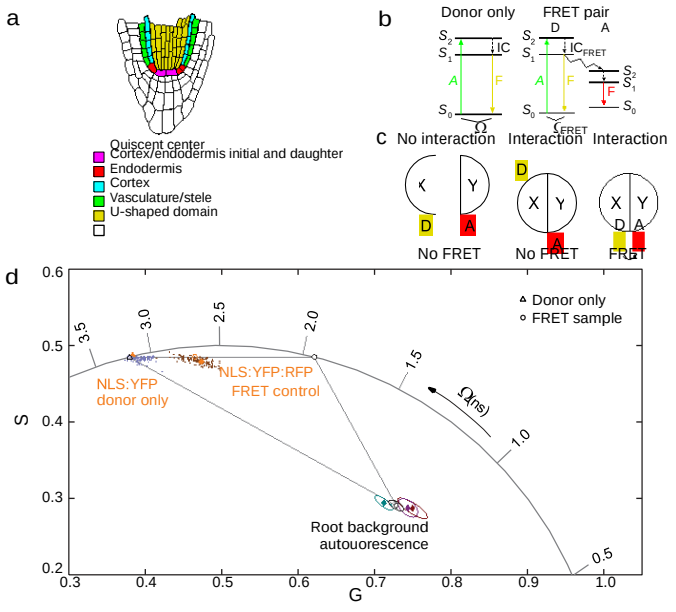

Figure 1 | Phasor analysis of *in vivo* FRET–FLIM. a, Schematic representation of the *Arabidopsis* root. **b**, Jablonski diagram depicting FRET. *A*, absorption; A, acceptor fluorophore; D, donor fluorophore; IC, internal conversion; *F*, fluorescence; S_0–S_2, limits of electronic energy states; τ and τ_{FRET}, fluorescence lifetime. **c**, Schematic illustration of FRET between fusion proteins. X and Y, tested proteins. **d**, **e**, Phasor plot depicting: donor-only (filled white triangle), FRET positive control (filled orange circle and cloud) and its projected pure FRET component (empty orange circle), the theoretical maximal FRET (filled white circle), a FRET sample of roots co-expressing *pSCR::SCR:YFP* and *pSCR::RFP:SHR* (blue cloud) and background signals (filled diamonds). G and S represent the two coordinates of the phasor plot. **f**–**j**, Phasor plots depicting cell type-specific native FRET–FLIM status of tested protein pairs, filled triangles and circles representing fluorescence lifetimes of donor-only and FRET samples, respectively, in different cell types, colour scheme as in **a**. Orange arrows mark FRET-specific shifts, black arrows mark background. Ellipses represent the confidence intervals of measured cells. Number of technical and biological replicates can be found in Supplementary Tables 1–5.

[1]Plant Developmental Biology, Wageningen University and Research Centre, Droevendaalsesteeg 1, Wageningen 6708PB, The Netherlands. [2]Molecular Genetics, Department Biology, Utrecht University, Padualaan 8, Utrecht 3581CH, The Netherlands. [3]CEPLAS (Cluster of Excellence on Plant Sciences), and Institute for Developmental Genetics, Heinrich Heine University, Universitätsstraße 1, Düsseldorf 40225, Germany. [4]Center for Advanced Imaging, Heinrich Heine University, Universitätsstraße 1, Düsseldorf 40225, Germany. [5]Swammerdam Institute for Life Sciences, Section of Molecular Cytology, van Leeuwenhoek Centre for Advanced Microscopy, University of Amsterdam, Science Park 904, Amsterdam 1098 XH, The Netherlands. [6]Departamento de Bioquímica, UAM, Instituto de Investigaciones Biomédicas Alberto Sols, CSIC-UAM, Arturo Duperier 4, 28029 Madrid, Spain. †Present address: Laboratoire Reproduction et Développement des Plantes (RDP), Université Lyon, ENS de Lyon, UCB Lyon 1, CNRS, INRA, F-69342 Lyon, France.

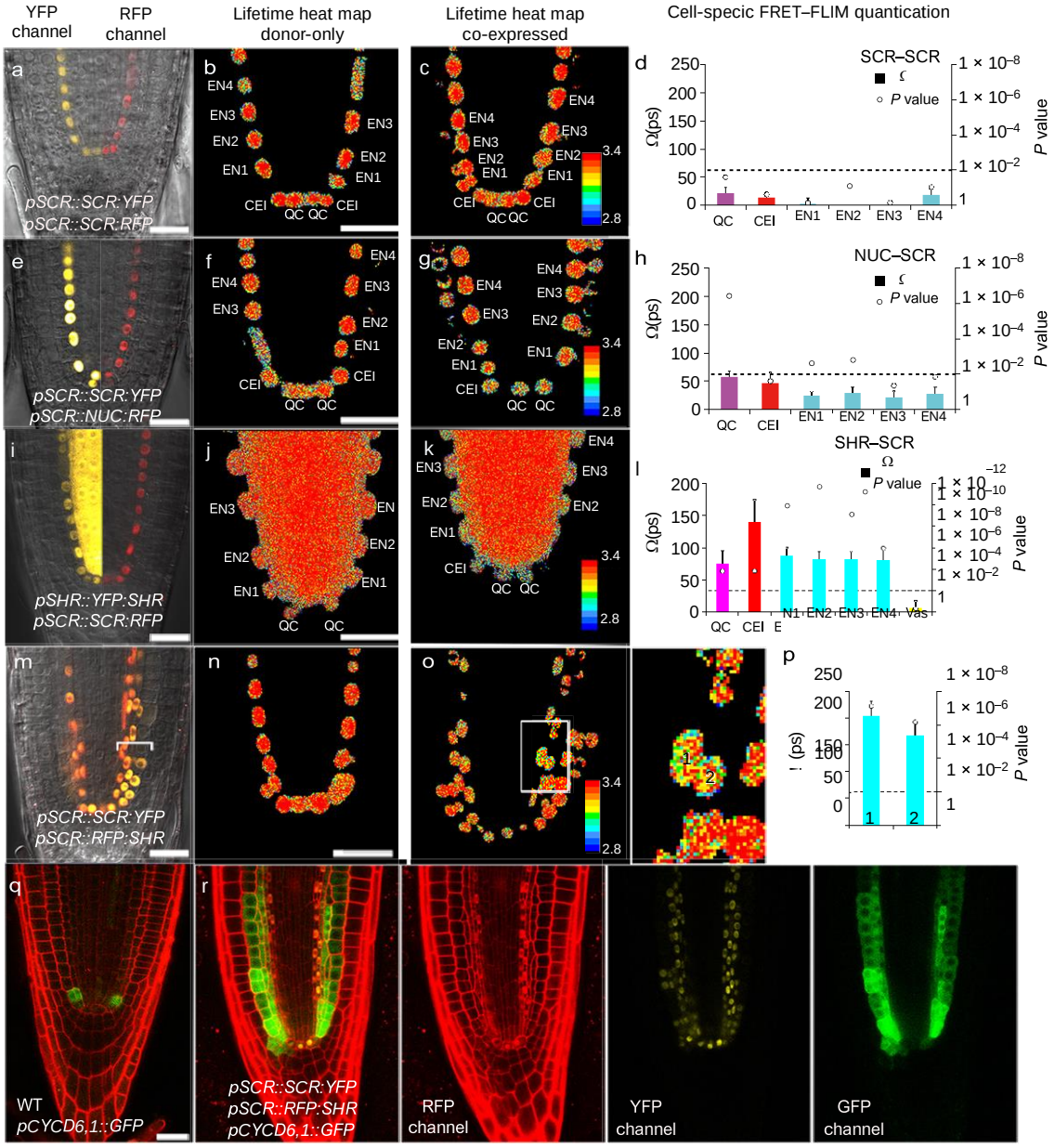

Figure 2 | FRET–FLIM quantification of SCR–SCR, NUC–SCR and SHR–SCR associations *in vivo*. **a**–**d**, *In vivo* FRET–FLIM analysis of roots co-expressing *pSCR::SCR:YFP* and *pSCR::SCR:RFP*. **a**, Co-localization of *pSCR::SCR:YFP* and *pSCR::SCR:RFP*, $n = 15$ roots. **b**, **c**, Fluorescence lifetime heat maps. **d**, Bar chart represents quantification of lifetime changes ($\Delta\tau$) in single cells. Error bars indicate standard errors. CEI, cortex/endodermis initial; EN1–4, first four endodermal cells; QC, quiescent centre; Vas, vasculature. Number of technical and biological replicates used for **b**–**d** can be found in Supplementary Table 1. **e**–**h**, *In vivo* FRET–FLIM analysis of roots co-expressing *pSCR::SCR:YFP* and *pSCR::NUC:RFP*. **e**, Co-localization of *pSCR::SCR:YFP* and *pSCR::NUC:RFP*; $n = 20$ roots. **f**, **g**, Fluorescence lifetime heat maps. **h**, The bar chart represents quantification of lifetime changes in single cells. Error bars, s.e. The number of technical and biological replicates for **f**–**h** can be found in Supplementary Table 2. **i**–**l**, *In vivo* FRET–FLIM measurement of roots co-expressing *pSHR::YFP:SHR* and *pSCR::SCR:RFP*. **i**, Co-localization, $n = 30$ roots. **l**, Quantification of lifetime change in single cells. Error bars, s.e. Number of technical and biological replicates used for **j**–**l** can be found in Supplementary Table 3. **m**–**p**, *In vivo* FRET–FLIM measurement of roots co-expressing *pSCR::SCR:YFP* and *pSCR::RFP:SHR*, showing induced extra formative division in endodermis (bracket). **m**, Co-localization, $n = 15$ roots. **n**, **o**, Fluorescence lifetime heat maps. Inset shows cells that originated from formative divisions, which are numbered 1 and 2 for their positions outside the vasculature. **p**, Quantifications of lifetime change of SCR:YFP in **o**. Error bars, s.e. Circles indicate *P* value calculated by Student's *t*-test comparing lifetimes of FRET sample to donor-only at each cell position, the dotted line marks the 0.01 significant value (**d**, **h**, **l**, **p**). Donor-only, EN nuclei number = 17. FRET sample cell 1 nuclei number = 10, cell 2 nuclei number = 13. **q**–**r**, Formative divisions in *pSCR::RFP:SHR* correlate with activation of *CYCD6;1*. **q**, *pCYCD6;1::GFP* localization in wild type, $n = 10$. **r**, *pCYCD6;1::GFP* in *pSCR::RFP:SHR* and *pSCR::SCR:YFP*, $n = 26$. Scale bars, 20 μm.

maintaining physiological protein activity judged by complementation (Extended Data Fig. 3).

To assess protein–protein interactions within individual root cell nuclei, we combined confocal imaging with single-pixel fluorescence lifetime acquisition[14], and generated lifetime phasor plots and pseudo-coloured lifetime heat maps (Supplementary Information).

Phasor points corresponding to QC and CEI shifted more to the auto-fluorescence phasors compared to other cell types, indicating

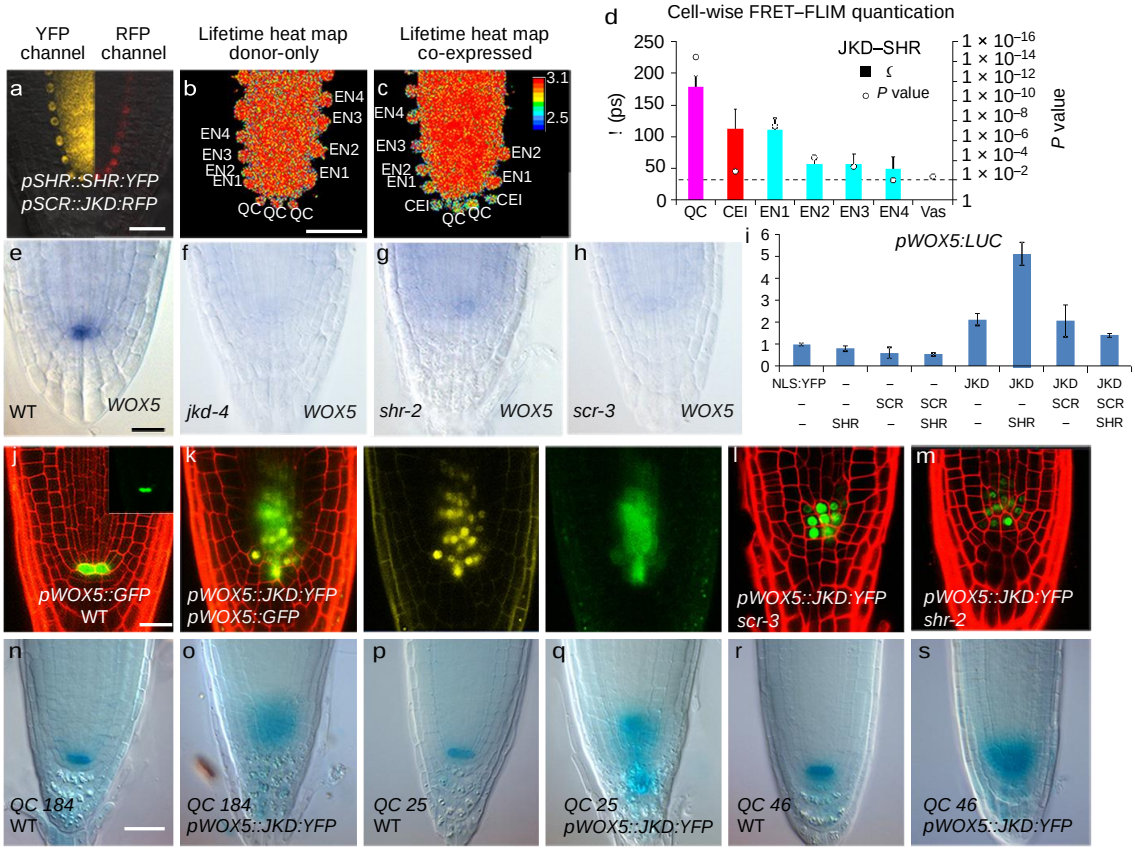

Figure 3 | FRET–FLIM analysis of JKD–SHR shows interaction in the QC and stem cells. a–d, *In vivo* FRET–FLIM measurements of roots co-expressing *pSHR::SHR:YFP* and *pSCR::JKD:RFP*. **a**, Co-localization, $n = 17$. **d**, Quantification of lifetime change in single cells. Error bars indicate standard errors. Circles indicate *P* value calculated by Student's *t*-test of sample lifetimes comparing lifetimes of FRET sample to donor-only at each cell position, with the dotted line marking the 0.01 significant value. Number of technical and biological replicates used in **b–d** can be found in Supplementary Table 4. Scale bars, 20 µm. **e–h**, JKD, SHR and SCR are required for *WOX5* activity, *in situ* hybridization showing *WOX5* RNA expression in wild type, $n = 24$ (**e**), *jkd*, $n = 18$ (**f**), *shr*, $n = 9$ (**g**) and *scr*, $n = 16$ roots (**h**). Scale bar, 10 µm. **i**, Dual-luciferase assay in *Nicotiana benthamiana* leaves. Experiments were performed three times and leaves transformation were done in triplicates. Error bars indicate standard deviations. **j–m**, JKD promotes *WOX5* activity independently from SCR and SHR. Confocal images of three-day-old roots expressing *pWOX5::GFP* in wild type, $n = 20$ (**j**), *pWOX5::JKD:YFP*, $n = 40$ (**k**), and *pWOX5::JKD:YFP* expression in *scr-3* mutant, $n = 15$ (**l**) and *shr-2*, $n = 12$ (**m**). **n–s**, Expansion of QC markers in *pWOX5::JKD:YFP*. QC184: $n = 7$ (**n**), $n = 24$ (**o**); QC25: $n = 6$ (**p**), $n = 7$ (**q**); QC46: $n = 8$ (**r**), $n = 7$ (**s**).

background influence with accompanying lifetime reduction in the stem cell niche (Fig. 1d–j). Nevertheless, FRET-specific donor lifetime reductions (shift to the right) were observed in SHR–SCR, JKD–SHR, and JKD–SCR combinations (Fig. 1h–j, Extended Data Table 1), indicating *in vivo* interaction. Cells expressing only donors, SHR in vasculature and JKD in cortex, lacked significant FRET-specific lifetime reduction (Fig. 1h–j, Extended Data Table 1), validating FRET specificity in the U-shaped domain.

In vivo FRET efficiency at physiological expression levels was low compared to overexpression, with maxima around 4%, but significant differences between cell types were still observed (Extended Data Table 1). Lifetime unmixing distinguished small lifetime reductions owing to FRET from higher relative auto-fluorescence levels at endogenous expression levels. To exclude bystander FRET, we studied non-interacting protein pairs expressed at similar levels as negative controls. We first quantified donor lifetime in roots co-expressing *pSCR::SCR:YFP* and *pSCR::SCR:RFP*, the established negative protein–protein interaction control[9], and found no substantial changes in SCR:YFP lifetime in the U-shape domain (Figs 1f, 2a–d, Extended Data Table 1, Extended Data Fig. 5). Additionally, limited to no *in vivo* FRET was detected in roots co-expressing SCR:YFP and the JKD homologue NUC:RFP under the *pSCR* promoter (Figs 1g, 2e–h, Extended Data Table 1), despite largely co-localizing in the U-shaped domain (Extended Data Fig. 5). These negative controls support that lifetime reduction by background auto-fluorescence does not hamper detection of FRET-specific lifetime reduction.

We next detected protein–protein interactions in plants co-expressing *pSHR::YFP:SHR* and *pSCR::SCR:RFP* (Fig. 2i, Extended Data Fig. 5). When expressed alone, the donor SHR:YFP signal exhibited a generally long lifetime depicted by the reddish pseudo-colour on the heat map (Fig. 2j); while a 'blue-shift' in the U-shaped domain, indicating lifetime reduction, appeared upon SCR:RFP co-expression (Fig. 2k). In contrast, lifetimes of the SCR–SCR and NUC–SCR pairs hardly changed (Fig. 2d, h, Extended Data Fig. 5), indicating that SHR–SCR lifetime reduction is probably due to protein–protein-interaction-specific FRET, consistent with the recently reported SHR–SCR association by fluorescence correlation spectroscopy[15]. Cell-specific quantification confirmed *in vivo* FRET of SHR–SCR and highlighted an increased lifetime reduction in CEI compared to QC and endodermal cells (Fig. 2l, Extended Data Table 1). In vasculature, where SHR:YFP was expressed without SCR, SHR:YFP fluorescence lifetime remained unchanged (Fig. 2l).

To test whether high SHR–SCR interaction in CEI correlated with formative divisions, we measured FRET in roots co-expressing *pSCR::SCR:YFP* and *pSCR::RFP:SHR* (Fig. 2m–p), in which ectopic *SHR* expression induces *SCR*-dependent formative endodermal divisions[8]. A substantial YFP lifetime reduction was associated with extra formative divisions and ectopic *CYCD6;1* expression (Fig. 2o–r),

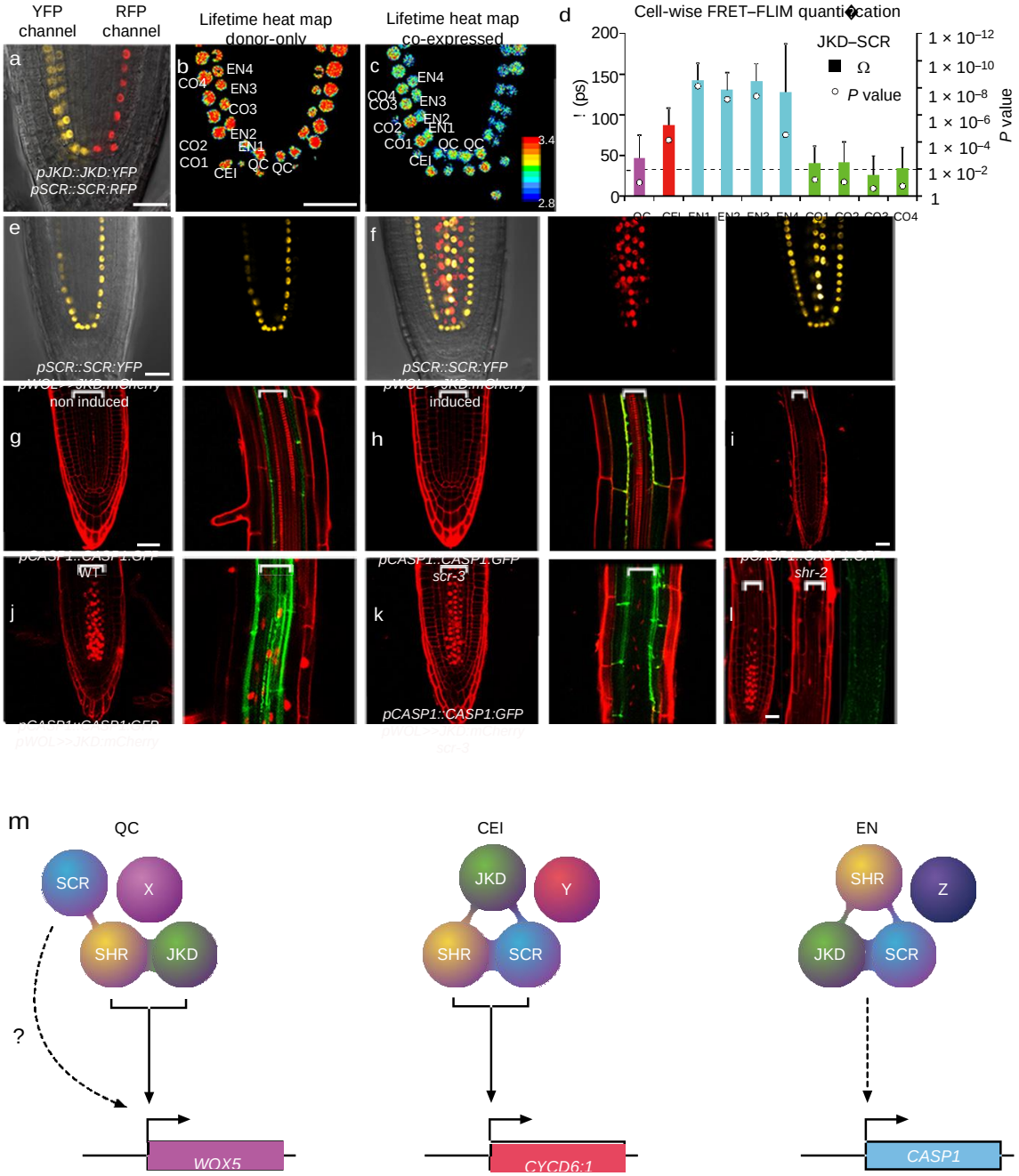

Figure 4 | FRET–FLIM analysis of JKD–SCR shows high interaction in endodermal cells. a–d, *In vivo* FRET–FLIM measurements in roots co-expressing *pJKD::JKD:YFP* and *pSCR::SCR:RFP*. **a**, Co-localization, $n = 20$. In **d**, Error bars indicate standard errors. Circles indicate *P* value calculated by Student's *t*-test of sample lifetimes comparing lifetimes of FRET sample to donor-only at each cell position, the dotted line marking the 0.01 significant value. Number of technical and biological replicates used in **b**–**d** can be found in Supplementary Table 5. **e**, **f**, Induction of *pWOL>>JKD:mCherry* activates *pSCR::SCR:YFP* expression in the vasculature ($n = 15$). **g**–**l**, Confocal images of roots expressing *pCASP1::CASP1:GFP*, in wild type, $n = 15$ (**g**), *scr*, $n = 7$ (**h**), *shr*, $n = 11$ (**i**), *pWOL>>JKD:mCherry* in wild type, $n = 20$ (**j**), *scr*, $n = 10$ (**k**) and *shr* mutants, $n = 9$ (**l**). Brackets mark vasculature. Scale bars, 20 µm. **m**, Scheme illustrating the effects of changes in the SCR–SHR–JKD complex conformation on target promoter activities and different cell fate specifications (QC, CEI, EN) as outputs. CEI, cortex/endodermis initial; EN, endodermis; QC, quiescent centre.

confirming the correlation between formative division and elevated SHR–SCR association.

Subsequently, we monitored lifetime distribution changes in roots co-expressing *pSHR::SHR:YFP* and *pSCR::JKD:RFP* (Fig. 3a, Extended Data Fig. 5). SHR:YFP lifetime significantly decreased in QC and CEI nuclei in the presence of JKD:RFP, visible by a blue-shift in the heat map (Fig. 3c), indicating that JKD–SHR association is enhanced within the stem cell niche. Cell-by-cell quantification verified high SHR:YFP lifetime reduction in the QC, moderate in the CEI, and low in the endodermis (Fig. 3d, Extended Data Table 1).

In the QC of *jkd* mutants, *WUSCHEL RELATED HOMEOBOX 5* (*WOX5*) transcript levels decreased markedly (Fig. 3e–h), indicating that *JKD*, like *SHR* and *SCR*, is essential for maintaining QC-specific *WOX5* expression[16,17]. *WOX5* is also weakly expressed in vascular stem cells[18] (Extended Data Figs 6, 7). We made use of this feature and ectopically expressed JKD under *pWOX5*, which amplifies *pWOX5* activity in vasculature (Fig. 3j–k, Extended Data Fig. 6). Such vascular cells displayed morphological changes (Extended Data Fig. 6) and expressed additional QC markers (Fig. 3n–s), indicating that ectopic *JKD* can promote QC fate acquisition. Notably, amplified *pWOX5* activity was still observed in *scr* and *shr* mutants (Fig. 3l, m), suggesting

that *JKD* can maintain and amplify *WOX5* expression independently of *SCR* and *SHR*. As *JKD* acts downstream of *SCR* and *SHR*[19], the increased *WOX5* expression in their absence can be interpreted as a transcriptional readout of *JKD*[7]. Nevertheless, promoter assays revealed that, among JKD/SHR/SCR combinations, JKD–SHR was most efficient in boosting *pWOX5* activity (Fig. 3i). Together with the early embryonic *WOX5* activation (Extended Data Fig. 6), this indicates that a specific physical association of JKD and SHR elevates *WOX5* activity under physiological conditions, while excessive JKD alone can maintain *WOX5* transcription. Collectively, our data indicate that QC-specific JKD–SHR interaction, as measured by FRET–FLIM, contributes to QC specification and maintenance.

The JKD–SCR association under endogenous promoters in roots revealed enriched FRET in endodermis, moderate in CEI and largely reduced in the QC (Fig. 4a–d). A close association of JKD with SHR, SCR or both is consistent with its role in promoting *SCR* expression to reinforce SHR nuclear retention while repressing formative divisions in the QC and endodermis[5]. The cell-specific segregation of JKD–SHR and JKD–SCR lifetime distribution suggests that, although close association of JKD with SHR links to QC function, close proximity to SCR may guide endodermal fate specification. To test this hypothesis, we misexpressed *JKD* in the procambial vasculature under the *WOODENLEG* promoter (*pWOL*)[20,21], which also activates local *SCR* misexpression[5] (Fig. 4e–f, Extended Data Fig. 7). In *pWOL>>JKD:mCherry* roots, the marker for mature root endodermis CASPARIAN STRIP MEMBRANE DOMAIN PROTEIN 1 (CASP1)[22] was induced in the vasculature (Fig. 4j), supporting that enriched JKD–SCR interaction is required for endodermal fate. Fate specification could involve JKD–SCR as a heterodimer or as a specific conformation of a multimeric complex. We therefore tested whether JKD-mediated *CASP1* misexpression required *SCR* or *SHR* by introgressing *pWOL>>JKD:mCherry* and *pCASP1::CASP1:GFP* co-expression lines into *scr* and *shr* mutants. This abolished vascular *CASP1* expression (Fig. 4 k–l), indicating that JKD–SCR confers endodermal fate in a SHR-dependent manner (Supplementary Discussion).

Our *in vivo* FRET–FLIM analysis indicates either distinct heterodimers or distinct conformations of SHR–SCR–JKD complexes within the U-shaped domain. To distinguish both options without interference of endogenous plant-specific factors, we performed split luciferase (split-LUC) competition assays in mammalian HeLa cells. SHR and SCR interacted strongly in HeLa cells, whereas JKD markedly reduced the SHR–SCR protein–protein interactions (Extended Data Fig. 8), indicating that JKD alters SHR–SCR interaction. Similarly, SHR–SCR association was reduced by RETINOBLASTOMA-RELATED (RBR) protein[23]. SHR–SCR interaction remained unaltered upon addition of free mCherry, free YFP or GFP-tagged human tumour suppressor protein p53 (Extended Data Fig. 8). JKD–SHR and JKD–SCR interaction was weaker than SHR–SCR in HeLa cells, implying that JKD requires plant-specific facilitators to strongly bind SHR and SCR. SCR promoted JKD–SHR interaction, and SHR boosted JKD–SCR association (Extended Data Fig. 8), suggesting preferential JKD binding to SHR–SCR complexes. Consistent with *in vivo* FRET, SCR did not associate with itself or NUC in HeLa cells (Extended Data Fig. 8). Together with co-immunoprecipitation from transiently expressing tobacco leaves, this demonstrates that SHR–SCR–JKD form a ternary complex (Extended Data Fig. 8), consistent with recent structural data of SHR, SCR and JKD[24].

Our *in vivo* FRET–FLIM analysis reveals that SHR, SCR and JKD form qualitatively different higher-order transcription factor complexes. These distinct complexes associate with target promoter selectivity and cell-fate segregation between closely neighbouring cells. Recent work showed that SHR exhibits different diffusion rates between tissue layers[15], supporting our data on distinct SHR complexes controlling its motility and dictating distinct cell fates (Fig. 4m, Extended Data Fig. 9, Supplementary Discussion). Combining fluorescence-correlation-spectroscopy-based techniques, which detect protein associations in bigger complexes, and *in vivo* FRET–FLIM with potentially enhanced nanometer-scale displacement detection using more complete-maturating monomeric red fluorescent protein 'mScarlet'[25] as a FRET acceptor, will allow precise monitoring of *in vivo* multiprotein complex dynamics. The next challenge will be to decipher mechanisms that generate diversity of protein–protein-interaction patterns to control target gene activation.

Online Content Methods, along with any additional Extended Data display items and Source Data, are available in the online version of the paper; references unique to these sections appear only in the online paper.

received 21 September 2016; accepted 19 June 2017.
Published online 26 July 2017.

1. Lemon, B. & Tjian, R. Orchestrated response: a symphony of transcription factors for gene control. *Genes Dev.* **14,** 2551–2569 (2000).
2. Spitz, F. & Furlong, E. E. M. Transcription factors: from enhancer binding to developmental control. *Nat. Rev. Genet.* **13,** 613–626 (2012).
3. Ladam, F. & Sagerström, C. G. Hox regulation of transcription: more complex(es). *Dev. Dyn.* **243,** 4–15 (2014).
4. Long, Y., Scheres, B. & Blilou, I. The logic of communication: roles for mobile transcription factors in plants. *J. Exp. Bot.* **66,** 1133–1144 (2015).
5. Long, Y. *et al. Arabidopsis* BIRD zinc finger proteins jointly stabilize tissue boundaries by confining the cell fate regulator SHORT-ROOT and contributing to fate specification. *Plant Cell* **27,** 1185–1199 (2015).
6. Sparks, E., Wachsman, G. & Benfey, P. N. Spatiotemporal signalling in plant development. *Nat. Rev. Genet.* **14,** 631–644 (2013).
7. Moreno-Risueno, M. A. *et al.* Transcriptional control of tissue formation throughout root development. *Science* **350,** 426–430 (2015).
8. Nakajima, K., Sena, G., Nawy, T. & Benfey, P. N. Intercellular movement of the putative transcription factor SHR in root patterning. *Nature* **413,** 307–311 (2001).
9. Cui, H. *et al.* An evolutionarily conserved mechanism delimiting SHR movement defines a single layer of endodermis in plants. *Science* **316,** 421–425 (2007).
10. Sozzani, R. *et al.* Spatiotemporal regulation of cell-cycle genes by SHORTROOT links patterning and growth. *Nature* **466,** 128–132 (2010).
11. Verveer, P. J. & Hanley, Q. S. in *Laboratory Techniques in Biochemistry and Molecular Biology* (ed. Gadella, T.W.J.) Vol. 33, 59–94 (Elsevier, 2009).
12. Gerritsen, H. C., Agronskaia, A. V., Bader, A. N. & Esposito, A. in *Laboratory Techniques in Biochemistry and Molecular Biology* (ed. Gadella, T. W. J.) Vol. 33, 95–132 (Elsevier, 2009).
13. Gadella, T. W. J. Jr, Jovin, T. M. & Clegg, R. M. Fluorescence lifetime imaging microscopy (FLIM): spatial resolution of microstructures on the nanosecond time scale. *Biophys. Chem.* **48,** 221–239 (1993).
14. Stahl, Y. *et al.* Moderation of *Arabidopsis* root stemness by CLAVATA1 and *ARABIDOPSIS* CRINKLY4 receptor kinase complexes. *Curr. Biol.* **23,** 362–371 (2013).
15. Clark, N. M. *et al.* Tracking transcription factor mobility and interaction in *Arabidopsis* roots with fluorescence correlation spectroscopy. *eLife* **5,** e14770 (2016).
16. Sarkar, A. K. *et al.* Conserved factors regulate signalling in *Arabidopsis thaliana* shoot and root stem cell organizers. *Nature* **446,** 811–814 (2007).
17. Sabatini, S., Heidstra, R., Wildwater, M. & Scheres, B. SCARECROW is involved in positioning the stem cell niche in the *Arabidopsis* root meristem. *Genes Dev.* **17,** 354–358 (2003).
18. Pi, L. *et al.* Organizer-derived WOX5 signal maintains root columella stem cells through chromatin-mediated repression of CDF4 expression. *Dev. Cell* **33,** 576–588 (2015).
19. Welch, D. *et al. Arabidopsis* JACKDAW and MAGPIE zinc finger proteins delimit asymmetric cell division and stabilize tissue boundaries by restricting SHORT-ROOT action. *Genes Dev.* **21,** 2196–2204 (2007).
20. Vatén, A. *et al.* Callose biosynthesis regulates symplastic trafficking during root development. *Dev. Cell* **21,** 1144–1155 (2011).
21. Bonke, M., Thitamadee, S., Mähönen, A. P., Hauser, M.-T. & Helariutta, Y. APL regulates vascular tissue identity in *Arabidopsis*. *Nature* **426,** 181–186 (2003).
22. Roppolo, D. *et al.* A novel protein family mediates Casparian strip formation in the endodermis. *Nature* **473,** 380–383 (2011).
23. Cruz-Ramírez, A. *et al.* A bistable circuit involving SCARECROW–RETINOBLASTOMA integrates cues to inform asymmetric stem cell division. *Cell* **150,** 1002–1015 (2012).
24. Hirano, Y. *et al.* Structure of the SHR–SCR heterodimer bound to the BIRD/IDD transcriptional factor JKD. *Nat. Plants* **3,** 17010 (2017).
25. Bindels, D. S. *et al.* mScarlet: a bright monomeric red fluorescent protein for cellular imaging. *Nat. Methods* **14,** 53–56 (2017).

Supplementary Information is available in the online version of the paper.

Acknowledgements We thank P. Benfey for discussions and critical reading of the manuscript, A. Akhmanova and B. P. Bouchet for providing mammalian cells lines and laboratory facilities to perform transfection assays, S. Diaz for sharing DLR protocols used in this study. This work was supported by an NWO VIDI grant to I.B. and Y.L. Y.L. was further supported by ERC Advanced Grant SysArc and NWO Spinoza Grant to B.S. M.P. was supported by an NWO ALW-VIDI grant 864.09.015 and S.W.P. was supported by DFG-project WE 5343/1-1.

Author Contributions The scientific concept was developed by I.B. and B.S. I.B. and Y.L. designed and executed the experiments. Y.L. generated constructs and lines used for FRET–FLIM experiments, I.B. and Y.L. performed the FRET–FLIM measurement in roots. Y.S., S.W.-P. and R.S. assisted in setting up, optimizing FRET–FLIM devices, data acquisition and analysis in living roots. M.P. performed and quantified the phasor analysis. J.G. helped Y.L. with FRET–FLIM measurements, optimization in protoplast and data analysis and interpretation. T.W.G.J. helped with phasor analysis and discussions related to FRET–FLIM quantification. W.Z. conducted co-immunoprecipitation experiments. Y.L. generated transgenic lines in wild-type and mutant background. I.B. performed DLR luciferase experiments, gene expression analysis by *in situ* hybridizations, reporter assays and phenotypic analysis in transgenic lines and mutant backgrounds. I.B., Y.L. and B.S. wrote the manuscript. M.-I.S.-P. contributed to HeLa cell experiments by sharing published materials and protocols. I.B., Y.L., B.S., Y.S., S.W.-P., R.S., W.Z., M.P., J.G. and T.W.G.J. contributed to data analysis, interpretation and revision of the manuscript.

Author Information Reprints and permissions information is available at www.nature.com/reprints. The authors declare no competing financial interests. Readers are welcome to comment on the online version of the paper. Publisher's note: Springer Nature remains neutral with regard to jurisdictional claims in published maps and institutional affiliations. Correspondence and requests for materials should be addressed to I.B. (ikram.blilou@wur.nl).

reviewer Information *Nature* thanks T. Beeckman and the other anonymous reviewer(s) for their contribution to the peer review of this work.

MethOdS

Data reporting. No statistical methods were used to predetermine sample size. The experiments were not randomized and the investigators were not blinded to allocation during experiments and outcome assessment.

Cloning. Coding sequences (CDS) of *mRFP* and *SYFP2*[26–28] were subcloned into multiple Gateway cassettes with flanking attB sites. A general SV40 nuclear localizing signal (*NLS*)[29] was attached to the N terminus of *SYFP2* to generate *NLS-SYFP2*. For C-terminal tagging, fluorescent protein sequences were recombined into pGEMTeasyR2R3 vector by Gateway BP reaction, and pGEMTeasy221-derived entry clones were generated for N-terminal tagging. *SHR*, *SCR*, *JKD* and *NUC* coding sequences in pDONR221-derived entry clones[5,19] were used for C-terminal tagging clones, and, for N-terminal tagging, *SHR* and *SCR* were subcloned into pGEMTeasyR2R3.

For protoplast transfection and *Arabidopsis* root FRET–FLIM control, the constitutive cauliflower mosaic virus *35S* promoter-driven fusion constructs with N- or C-terminal tagging were created in pB7m34GW or pH7m34GW binary vectors[30] by multiple Gateway LR reactions (Invitrogen). Vectors for root expression analysis of tested proteins were created similarly with endogenous promoters[5]. For a functional *SYFP2:SHR* construct, *pSHR::SYFP2:SHR* with four amino acids linker was generated by site-directed mutagenesis (QuikChange II, Aligent) from *pSHR::SYFP2:SHR* Gateway vector. For *in vivo* FRET–FLIM measurement of JKD–SHR and NUC–SCR combinations, the endogenous BIRD promoters were too weak for sufficient FRET measurement. Therefore the expression of BIRD proteins was enhanced in the U-shaped domain using the *SCR* promoter.

Plasmids for bimolecular fluorescence complementation assay in protoplasts are as described in ref. 5.

For split-LUC assay in HeLa cells, vectors were generated from HeLa expression vectors described in ref. 5 by substituting the fluorescence protein tag with N- or C-ternimal half of *Renilla LUC* (*NrLUC* or *CrLUC*). A linker of 2× Gly-Gly-Gly-Gly-Ser was introduced between *CDS* and *rLUC* halves, except for *NrLUC-SHR* in which a Gly-Tyr-Lys linker was used. Primers used for cloning and constructs used in this study are listed in the Supplementary Information.

***Arabidopsis* growth condition and transformation.** *Arabidopsis thaliana* ecotype Columbia (Col-0) plants containing fusions constructs were grown as in ref. 5. Stably transformed lines were generated by *Agrobacterium tumefaciens*-mediated transformation via floral dip method[31]. Plants containing FRET–FLIM pairs were generated by crossing.

Bimolecular fluorescence complementation assay in protoplasts. *Arabidopsis* leaf mesophyll protoplasts were prepared and transfected according to ref. 5. Transfection was performed with 1 µg of each plasmid, and cells were observed after overnight incubation.

Transient split-LUC assay in HeLa cells. HeLa cells lines used in this study were described in ref. 32 and were routinely checked for mycoplasma contamination using LT07-518 Mycoalert assay (Lonza).

Cells were transfected with 20 ng *fLUC* control, 100 ng *NrLUC* fusion, 100 ng *CrLUC* fusion and 300 ng competitor according to ref. 5. Vectors used are as followed: *NrLUC-SHR* and *SCR-CrLUC* for SHR–SCR interaction; *SHR-NrLUC* and *CrLUC-JKD* for JKD–SHR interaction; *SCR-NrLUC* and *CrLUC-JKD* for JKD–SCR interaction. Constitutively expressed free mCherry, free SYFP2, SYFP2:SHR, SCR:mCherry, JKD:SYFP2, NUC:mCherry, p53:GFP and RBR:SYFP2 were used as competitors. Luciferase activities were measured by using the Dual-Luciferase Reporter Assay System in a GloMax 96 Microplate Luminometer (Promega). The obtained LUC levels were normalized using Firefly luciferase, and the relative ratio was determined by comparing this to those obtained with the single-transfected NrLUC fusion samples as described in ref. 23.

Confocal microscopy and image processing. Confocal microscopy was performed using a Zeiss LSM710, a Leica SP2 or a Leica SP8 confocal, as described in ref. 6 with the same spectrum settings.

Embryos and mature embryos were isolated from ovules and seeds, respectively, before staining with periodic acid–Schiff, as described in ref. 33. Samples were mounted in Hoyer solution before imaging.

For roots expressing fluorescent proteins, samples were mounted either in water or in 10 µM of propidium iodide.

Images were processed using Image Adobe Photoshop CS6 as follow: for Figs 2a, e, i, 3a and 4a, half of the image from the red channel of the same root was combined with the complementary half of the yellow channel to show protein colocalization. Confocal images of roots were rotated to have vertical orientation and the resulting empty space was filled with black pixels to create rectangular panels in Fig. 4g, h, i, k. Contrast of confocal images was enhanced for improving fluorescence visualization, and roots were rotated to have a vertical orientation. The resulting empty space in FLIM heat maps outside the roots was filled with black pixels to create rectangular panels. For Figure 2r, images were corrected for drift.

Fluorescence intensity analysis in roots. The fluorescence intensity of *pSCR::SCR:YFP*, *pSHR::SHR:YFP*, *pJKD::JKD:YFP* and *pNUC::NUC:YFP* was determined using ImageJ software, on images acquired with a single in-focus plane using equal laser power, detector gain and pinhole. A region of interest (ROI) was drawn around each nucleus and the mean fluorescence was measured. One ROI per root was also selected in root regions without fluorescence signal for background subtraction. The obtained data were tested for normal distribution and then subjected to a Student's *t*-test.

Frequency-domain FRET–FLIM measurement in protoplasts. Living transfected protoplasts were collected in LabTek chambered coverglass (Nunc) for frequency-domain FLIM measurements. Samples with cyan fluorescent donors were acquired according to ref. 26 and samples with yellow fluorescent donor were acquired according to ref. 27. In brief, mTurquoise fluorescence was excited with a 440-nm modulated diode laser (LDH-M-C-440; PicoQuant) at 75.1 MHz, the light was reflected by a 455DCLP dichroic mirror and emission was passed through a D480/40 band-pass emission filter (Chroma Technology). SYFP2 fluorescence was excited with a 514 nm Argon laser (Melles-Griot) intensity-modulated at a frequency of 75.1 MHz and the light was reflected by a 525DCXR dichroic mirror and emission was passed through a HQ545/30 band-pass emission filter (Chroma Technology). Emission was detected using a radio-frequency-modulated image intensifier (Lambert Instruments II18MD) coupled to a charge-coupled device (CCD) camera (Photometrics HQ) as a detector. FLIM stacks of 18 phase images were acquired in permutated recording order with an exposure time of 50–1,000 ms per image depending on sample brightness. The average fluorescence lifetime of individual nuclei was quantified, and an average lifetime for the sample was determined from this. FRET efficiency was calculated as described in ref. 2. More than 25 cells were analysed for each sample.

Time-domain FRET–FLIM measurement in living *Arabidopsis*. Vertically grown primary roots of 3–4-day-old seedlings were mounted in water for measurements. Time-domain FLIM was performed on a confocal laser scanning microscope (Zeiss LSM 780) additionally equipped with a single-photon counting device with picosecond time resolution (PicoQuant Hydra Harp 400). SYFP2 and Venus fluorescence was excited at 485 nm using a linearly polarized diode laser (LDH-D-C-485) operated at a repetition rate of 32 MHz. Excitation power was around 1 µW at the objective (40× water immersion, Zeiss C-PlanApo, NA 1.2). The emitted light was collected in the same objective and separated into its perpendicular and parallel polarization (Thorlabs PBS 101, Thorlabs GmbH, Germany). Fluorescence was then detected by Tau-SPADs (PicoQuant) in a narrow range of YFP variants' emission spectrum (band-pass filter: HC535/30 AHF). Images were taken with 12.6 µs pixel time and a resolution of 0.1 µm per pixel (zoom 4 and 2, 256 × 256). A series of 60 frames were merged into one image and further analysed.

Data conversion for phasor plots. To extract intensity and lifetime information from the HydraHarp files an in-house written C++ program (Qt) was used. Header information and photon record processing was based on the code provided by PicoQuant. From each file and each channel (1–4), arrival times were converted to pixel positions and a stack of images was extracted. A binary file containing a list with coordinates and delay times (x, y, z, τ_d) for each photon was exported to construct decay curves at each pixel in the image.

Drift correction. In some datasets, drift was apparent during the acquisition. In order to correct for this drift, allowing a more accurate nucleus selection, each YFP stack containing 60 images was smoothed using a 3 × 3 × 3 box filter, and 11 key-frames were used spanning the whole stack. The global drift vector based on drift between all key frames was calculated and used to correct the pixel position of each photon in the dataset. In order to calculate the global drift vector for the 10 RFP images 3 key frames were used and the drift-corrected RFP channel was subsequently aligned to the drift-corrected YFP channel in order to align the RFP channel to the YFP channel.

Decay curve extraction and phasor analysis. Each corrected YFP image stack was summed and the resulting image was used for drawing regions of interests (ROIs) at nuclei of different cell types using imageJ. These ROIs were exported as ROI sets and imported in MATLAB. For each ROI the decay curve was extracted from the TIFF stack that contains the decay curves for each pixel.

Prior to calculation of phasors, each decay curve extracted from ROIs was fitted with an exponential decay model in order to estimate the background parameter (offset) and the position (shift) of the instrument response function (IRF). The decay was modelled with a sum of up to three exponential functions, which were reconvolved with the IRF that extracted from the control measurement only containing the YFP, and in which no acceptor was present. The IRF was estimated in multiple nuclei with high photon counts (>10^5 photons) using Richardson–Lucy deconvolution, assuming an YFP lifetime of 3.18 ns and the same technique used by PicoQuant, which uses the rising phase of the decay curve. All extracted IRFs from multiple nuclei were then aligned and averaged to obtain a consensus IRF. The general decay model, $h_k(t)$ used was:

$$h_k(t) = b_k + \mathrm{IRF}(t - t_{s,k}) \otimes \sum_i a_{k,i} \exp(-t/\tau)\Delta t/\tau$$

where Δt denotes the bin size of the decay curve (32 ps), b_k denotes the background parameter, $a_{k,i}$ denotes the amplitude parameter in total photon counts for component i, and τ_i denotes the lifetime of component i. The estimated shift of the IRF is denoted by $t_{s,k}$. The complex phasor points, $p_h = g_h(\omega) + is_h(\omega)$ were calculated using the cosine and sine transforms:

$$g_k(\omega) = \frac{\sum_j \cos(\omega t_j) h'_j}{\sum_j h'_j}$$

$$s_k(\omega) = \frac{\sum_j \sin(\omega t_j) h'_j}{\sum_j h'_j}$$

Where h'_j denotes the background corrected decay curve ($h'_j = h_j - b_k$) and ω the angular frequency, $\omega = 2\pi n/T$. We used the third harmonic $n = 2$ and the sample period was $T = 31.25$ ns, yielding an angular frequency of $\omega = 0.402$ rad ns^{-1}. In order to correct for the IRF the complex phasor points obtained from the measured decay curves was divided by the phasor of the shifted IRF, hence $p_h(\omega) = p_h(\omega) / p_{\mathrm{IRF}}(\omega)$.

From multiple decay curves, the weighted mean phasor point was calculated, where the total number of photons in the decay curve was used as the weight. The 2D equivalent of the Studentized bootstrap technique was used in order to calculate the confidence ellipses of the weighted mean. In total, $N = 1{,}000$ bootstrap datasets were randomly selected from the original set, and the number of photons in the decay curve determined the probability of randomly selecting a phasor point (Monte Carlo). In this way 1,000 weighted means were obtained per set. The 95% ($\alpha = 0.95$) confidence ellipses were calculated from these bootstrap values by using a principal component analysis to obtain the eigenvectors (orientation of the ellipse) and for the size of the confidence ellipse ($r_{1,2}$) the eigenvalues ($\lambda_{1,2}$) and the inverse F-distribution was used ($r_{1,2} = \sqrt{\lambda_{1,2} F^{-1}(\alpha, 2, N-2)(N-1)/(N-2)}$).

Single-pixel fluorescence lifetime analysis. The fluorescence lifetime of SYFP2 and Venus was determined and analysed pixel-wise in merged images to increase photon numbers for analysis using the software tools 'AnI-3SF' and 'Margarita' developed by the C. A. M. Seidel group (Software Package for Multiparameter Fluorescence Spectroscopy, Full Correlation and Multiparameter Fluorescence Imaging (http://www.mpc.uni-duesseldorf.de/seidel)) for Multiparameter Fluorescence Image Spectroscopy (MFIS)[34,35]. In fluorescence lifetime microscopy with high spatial resolution and low excitation power to prevent photo bleaching, the number of photons per pixel is low, ranging from 100 to 2,000 photons per pixel. Therefore, a model to fit the data with a minimal number of parameters has to be applied in conjunction with a maximum likelihood estimator (MLE)[35–39]. The decay of SYFP2 and Venus is approximated in the subsequent fluorescence lifetime analysis by an average lifetime, τ. We therefore used a monoexponential model function with two variables (fluorescence lifetime τ and scatter contribution γ; as described elsewhere[14]), fitted with maximum likelihood estimator. The instrument response function was measured using the dye erythrosine, which exhibits a very short fluorescence lifetime, which is additionally quenched in an aqueous, saturated potassium iodide solution. This approach delivers the average fluorescence lifetime as a stable parameter even in critical surroundings with high background and low expression levels.

Cell-type-specific FRET–FLIM quantification. Roots with clear in-focus plane where cell types could be easily identified and with clear nuclei were used for lifetime quantifications.

Nuclear areas of no smaller than 25 pixels, based on the appearances of the nuclei after the 100-photon-per-pixel background subtraction, were selected from independent cells. The average fluorescence lifetime per cell was computed by fitting the lifetime distribution of each cell to a Gaussian model. Average fluorescence lifetimes at the same cell position were pooled from independent measurements without normalization, enabled by the robust FRET–FLIM acquisition between samples and between experiments. Reduction of fluorescence lifetime between donor-only and FRET samples were calculated from the means of donor-only and FRET samples at each cell position, with inclusion of fractional standard errors. Significances, between donor-only and FRET samples at specific cell positions in the same or different experiments, were resolved by Student's t-test with critical value of $P < 0.01$.

***In situ* hybridization.** For *WOX5* expression, whole-mount *in situ* hybridizations were performed using two-day-old seedlings as described in refs 16, 40.

Co-immunoprecipitation. The co-immunoprecipitation experiments were performed according to published procedure[41]. In brief, *Agrobacterium* with binary vectors containing CDS of *SCR*, *SHR:YFP* and *JKD-myc* were infiltrated into *N. benthamiana* leaves. The infiltrated leaf tissues were collected, ground in liquid nitrogen and resuspended in native extraction buffer (50 mM TRIS-MES pH 8.0, 0.5 M sucrose, 1 mM $MgCl_2$, 10 mM EDTA, 5 mM Dithiothreitol, protease inhibitor cocktail CompleteMini tablets (Roche)) on ice. Total extract was centrifuged at 16,000*g* at 4 °C for 15 min and protein complexes were captured using the uMACS GFP beads (Miltenyi Biotec) and c-myc beads (Santa Cruz).

For immunoblot analysis, proteins were separated by SDS–PAGE in a 10% acrylamide gel and electroblotted. Bands were detected with the Amersham ECL western blotting detection reagents (Amersham). Antibodies used in these experiments were as follows: anti-Myc antibody (sc-40, Santa Cruz), anti-GFP antibody (Roche), anti-SCR antibody (Santa Cruz), donkey anti-goat HRP-conjugated antibody, and goat anti-mouse HRP-conjugated antibody.

Data availability. All materials and datasets generated and analysed during the current study are available from the corresponding author upon reasonable request. The datasets for FRET–FLIM measurements plotted in Figs 2–4 and Extended Data Fig. 1 are available as Source Data files (raw data Figs 2–4; raw data Extended Data Fig. 1). Full scan gels can be found in the Supplementary Information. Sequence data from this article can be found in the *Arabidopsis* Genome Initiative or GenBank/EMBL databases under the following accession numbers: JACKDAW, AT5G03150; NUTCRACKER, AT5G44160; SCARECROW, AT3G54220; and SHORT-ROOT, AT4G37650.

26. Goedhart, J. *et al.* Bright cyan fluorescent protein variants identified by fluorescence lifetime screening. *Nat. Methods* **7,** 137–139 (2010).
27. Goedhart, J., Vermeer, J. E. M., Adjobo-Hermans, M. J. W., van Weeren, L. & Gadella, T. W. J. Jr. Sensitive detection of p65 homodimers using red-shifted and fluorescent protein-based FRET couples. *PLoS ONE* **2,** e1011 (2007).
28. Kremers, G.-J., Goedhart, J., van Munster, E. B. & Gadella, T. W. J. Jr. Cyan and yellow super fluorescent proteins with improved brightness, protein folding, and FRET Förster radius. *Biochemistry (Mosc.)* **45,** 6570–6580 (2006).
29. Lassner, M. W., Jones, A., Daubert, S. & Comai, L. Targeting of T7 RNA polymerase to tobacco nuclei mediated by an SV40 nuclear location signal. *Plant Mol. Biol.* **17,** 229–234 (1991).
30. Karimi, M., Bleys, A., Vanderhaeghen, R. & Hilson, P. Building blocks for plant gene assembly. *Plant Physiol.* **145,** 1183–1191 (2007).
31. Clough, S. J. & Bent, A. F. Floral dip: a simplified method for *Agrobacterium*-mediated transformation of *Arabidopsis thaliana*. *Cell. Mol. Biol.* **16,** 735–743 (1998).
32. Mimori-Kiyosue, Y. *et al.* CLASP1 and CLASP2 bind to EB1 and regulate microtubule plus-end dynamics at the cell cortex. *J. Cell Biol.* **168,** 141–153 (2005).
33. Truernit, E. *et al.* High-resolution whole-mount imaging of three-dimensional tissue organization and gene expression enables the study of phloem development and structure in *Arabidopsis*. *Plant Cell* **20,** 1494–1503 (2008).
34. Kudryavtsev, V. *et al.* Monitoring dynamic systems with multiparameter fluorescence imaging. *Anal. Bioanal. Chem.* **387,** 71–82 (2007).
35. Weidtkamp-Peters, S. *et al.* Multiparameter fluorescence image spectroscopy to study molecular interactions. *Photochem. Photobiol. Sci.* **8,** 470–480 (2009).
36. Schaffer, J. *et al.* Identification of single molecules in aqueous solution by time-resolved fluorescence anisotropy. *J. Phys. Chem. A* **103,** 331–336 (1999). 37.
Eggeling, C. *et al.* Data registration and selective single-molecule analysis using multi-parameter fluorescence detection. *J. Biotechnol.* **86,** 163–180 (2001). 38.
Widengren, J. *et al.* Single-molecule detection and identification of multiple species by multiparameter fluorescence detection. *Anal. Chem.* **78,** 2039–2050 (2006).
39. Sisamakis, E., Valeri, A., Kalinin, S., Rothwell, P. J. & Seidel, C. A. M. Accurate single-molecule FRET studies using multiparameter fluorescence detection. *Methods Enzymol.* **475,** 455–514 (2010).
40. Hejátko, J. *et al.* *In situ* hybridization technique for mRNA detection in whole mount *Arabidopsis* samples. *Nat. Protoc.* **1,** 1939–1946 (2006).
41. Liu, L. *et al.* An eficient system to detect protein ubiquitination by agroinfiltration in *Nicotiana benthamiana*. *Plant J. Cell Mol. Biol.* **61,** 893–903 (2010).

Extended Data Figure 1 | Cell-type organization and co-localization of key transcription factors in the *Arabidopsis* root meristem and FRET–FLIM determination in *Arabidopsis* protoplasts. a, Schematic illustration of the *Arabidopsis* root meristem, with marked tissue types (cell background colour) and co-localization pattern of SHR, SCR, JKD, NUC and *CYCD6;1* (circle colours). The U-shaped domain is encircled by a bold black line. QC, quiescent centre; CEI, cortex/endodermis initial; EN, endodermis; CO, cortex; Vas, vasculature. **b**, The SHR–SCR–JKD–NUC protein regulatory network (details and references can be found in the text). Red arrow, transcriptional activation; blue flat arrow, transcriptional repression; black line, protein–protein interaction. **c**, Bimolecular fluorescence complementation assays in *Arabidopsis* mesophyll protoplasts confirming interaction between SHR, SCR, JKD and NUC ($n > 20$). **d**, **e**, FRET quantification between SHR, SCR, JKD and NUC in protoplasts. E_{ϕ}, phase efficiency; E_{mod}, modulation efficiency. Error bars, standard errors (**d**, **e**). 28 cells were measured for N-SCR, 64 for SCR-C N-SHR; 53 for SCR-C SHR-C; 97 for N-SHR; 63 for N-SHR E2FA-C; 96 for SHR-C JKD-C; 99 for SHR-C N-JKD; 64 for SCR-C; 101 for SCR-C JKD-C; 95 for SCR-C N-JKD; 93 for SCR-C NUC-C; 66 for SCR-C N-NUC. N and C refer to the position of the fluorophore tagged either to the C terminus (C) or N terminus (N) of each protein. Source Data are available.

Extended Data Figure 2 | SHR and SCR complement their respective mutant phenotypes. a, Image of four-day-old seedlings of wild-type, *shr-2*, *pSHR::SHR:YFP* in wild-type, *pSHR::YFP:SHR* in *shr-2* and *35S::SHR:GFP*. 20 seedlings per genotype were plated. **b**–**g′**, Confocal images of three-day-old roots from seedlings of wild type, $n = 10$ (**b**, **b′**); *shr-2*, $n = 11$ (**c**, **c′**); *pSHR:YFP::SHR* in wild type, $n = 12$ (**d**, **d′**); *pSHR:YFP::SHR* in *shr-2*, $n = 11$ (**e**, **e′**); *pSHR::SHR:YFP* in wild type, $n = 16$ (**f**, **f′**); and *35S::SHR:GFP*, $n = 15$ (**g**, **g′**). **h**, Image of four-day-old seedlings of wild type, *scr-3*, *pSCR::SCR:YFP* in wild type, *pSCR::SCR:YFP* in *scr-3* and *35S::SCR:GFP*. 15 seedlings per genotype were plated. **i**–**m′**, Confocal images of three-day-old roots from seedlings of wild type, $n = 10$ (**i**, **i′**); *scr-3*, $n = 10$ (**j**, **j′**); *pSCR::SCR:YFP* in wild type, $n = 10$ (**k**, **k′**); *pSCR::SCR:YFP* in *scr-3*, $n = 11$ (**l**, **l′**); and *35S::SCR:GFP*, $n = 15$ (**m**, **m′**). Insets showing details of tissue layers. co, cortex; en, endodermis; ep, epidermis; mn, monolayer; sn, supernumerary layers; vas, vasculature. Scale bars, 20 μm.

Extended Data Figure 3 | Functional analysis of JKD and NUC protein fusions under endogenous and *SCR* promoters. a, Image of four-day-old seedlings of wild type, *pJKD::JKD:YFP* in wild type, *pSCR::JKD:YFP* in wild type, *pSCR::JKD:YFP* in *jkd-4* and *35S::JKD:YFP*. 20 seedlings per genotype were plated. **b**, Image of four-day-old seedlings of wild type, *jkd-4*, *pJKD::JKD:YFP* in wild type, *pJKD::JKD:YFP* in *jkd-4*. 15 seedlings per genotype were plated. **c**–**j**, Confocal images of three-day-old roots from seedlings of wild type, $n = 10$ (**c**, **c′**); *jkd-4*, $n = 12$ (**d**, **d′**); *pJKD::JKD:YFP* in wild type, $n = 12$ (**e**, **e′**); *pJKD::JKD:YFP* in *jkd-4*, $n = 10$ (**f**, **f′**); *pSCR::JKD:YFP* in wild type, $n = 8$ (**g**, **g′**); *pSCR::JKD:YFP* in *jkd-4*, $n = 7$ (**h**, **h′**); wild type, $n = 7$ (**i**) and *35S::JKD:YFP*, $n = 14$ (**j**). Insets showing details of tissue layers. **k**, Image of four-day-old seedlings of wild type; *pNUC::NUC:YFP* in wild type; *pSCR::NUC:YFP* in wild type and *35S::NUC:YFP*. 20 seedlings per genotype were plated. **l**–**o**, Confocal images of three-day-old roots from seedlings of *pNUC::NUC:YFP* in wild type, $n = 10$ (**l**, **l′**); *pSCR::NUC:YFP* in wild type, $n = 10$ (**m**, **m′**); wild type, $n = 10$ (**n**); and *35S::NUC:mCherry*, $n = 24$ (**o**). Insets show details of tissue layers. co, cortex; en, endodermis; ep, epidermis; pe, pericycle; vas, vasculature. Arrow points to elongated cells exiting the meristem. Scale bars, 20 µm.

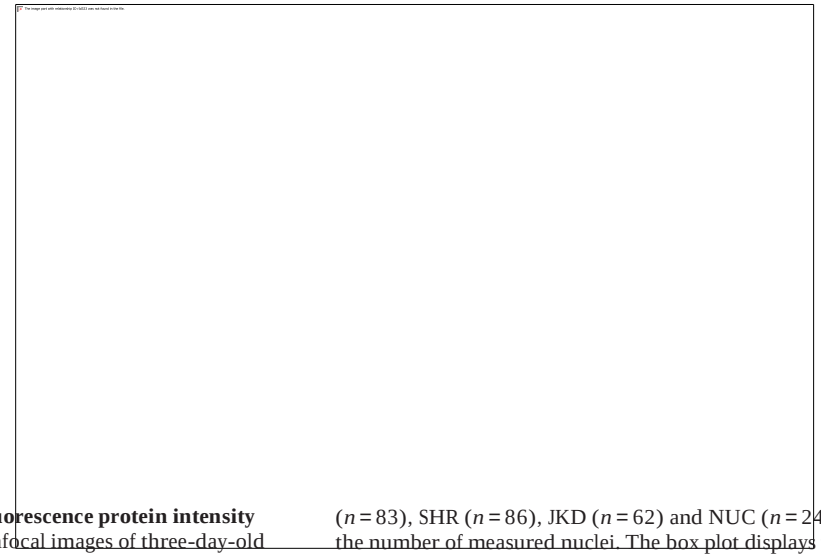

Extended Data Figure 4 | Analysis of fluorescence protein intensity under endogenous promoters. a–d, Confocal images of three-day-old roots from seedlings of *pSCR::SCR:YFP*, *pSHR:SHR:YFP*, *pJKD::JKD:YFP* and *pNUC::NUC:YFP*. Scale bar, 20 µm. **e**, Box plots showing differences in YFP intensity (16-bit) of roots expressing endogenous fusions of SCR ($n = 83$), SHR ($n = 86$), JKD ($n = 62$) and NUC ($n = 24$). *n* represents the number of measured nuclei. The box plot displays the distribution of fluorescence intensity: median, 1st and 3rd quartiles, minimum and maximum. The error bars indicate minimum and maximum of distribution.

Extended Data Figure 5 | Panels of donor fluorescence lifetime and fluorescence intensity of YFP and RFP channels of all protein pairs used in this study. All heat maps are the same ones used in Figs 2–4 with the same colour scale. YFP and RFP channel intensity images of the same roots are next to the heat maps displayed in Figs 2–4. Number of technical and biological replicates can be found in Supplementary Tables 1–5.

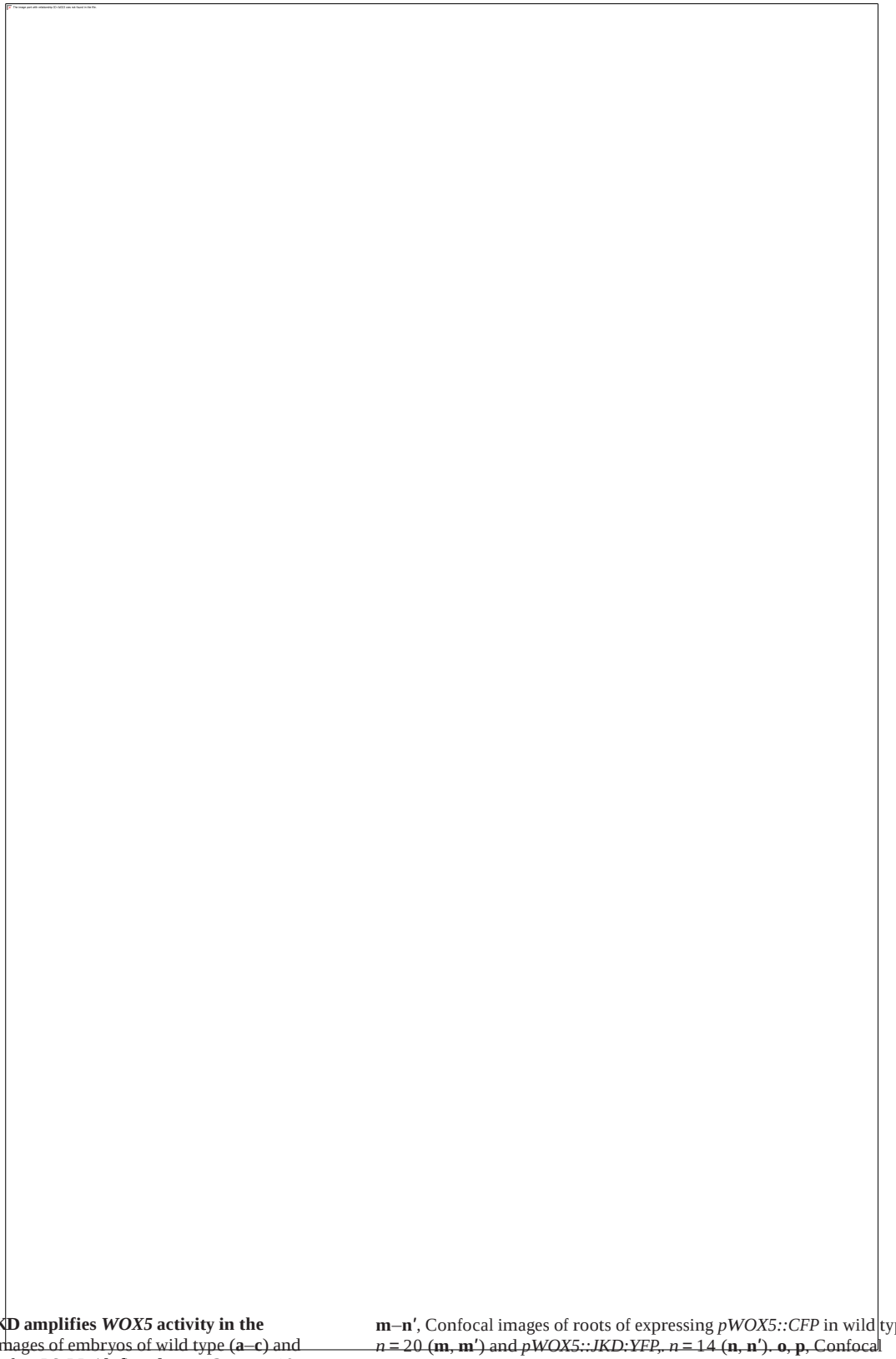

Extended Data Figure 6 | JKD amplifies *WOX5* activity in the vasculature. a–**f**, Confocal images of embryos of wild type (**a**–**c**) and *pWOX5::JKD:YFP* stained with mPS-PI. (**d**–**f**). **a**, **b**, $n = 13$; **c**, $n = 10$; **d**, **e**, $n = 35$; **f**, $n = 22$. **g**–**i**, Confocal images of embryos expressing *pWOX5::CFP*, $n = 14$. **j**–**l**, Confocal images of embryos expressing *pWOX5::JKD:YFP*, $n = 15$. Scale bars, 10 µm (**a**–**j**, **k**), 50 µm (**l**). **m**–**n′**, Confocal images of roots of expressing *pWOX5::CFP* in wild type, $n = 20$ (**m**, **m′**) and *pWOX5::JKD:YFP*, $n = 14$ (**n**, **n′**). **o**, **p**, Confocal images of roots of wild type, $n = 10$ (**o**) and *pWOX5::JKD:YFP*, $n = 8$ stained with mPS-PI (**p**). **q**, **r**, *In situ* hybridization showing *WOX5* mRNA expression in wild type, $n = 27$ (**q**) and *pWOX5::JKD:YFP*, $n = 29$ (**r**). Scale bars, 20 µm (**m**–**r**).

Extended Data Figure 7 | JKD expression in the vasculature does not affect *WOX5* activity. a, **b**, Confocal images of roots of wild type, $n = 10$ (**a**) and *pWOL>>JKD:mCherry*, $n = 13$ (**b**) stained with mPS-PI. Scale bars, 10 µm. **c**, **d**, *In situ* hybridization showing *WOX5* mRNA expression in wild type, $n = 20$ (**c**) and *pWOL>>JKD:mCherry*, $n = 32$ (**d**). Scale bars, 20 µm. **e**–**f′**, Confocal images of roots expressing *pWOX5::CFP* in wild type, $n = 22$ (**e**, **e′**) and in *pWOL>>JKD:mCherry*, $n = 27$ (**f**, **f′**). Scale bars, 10 µm.

Extended Data Figure 8 | SHR, SCR and JKD form ternary complex. **a**–**d**, Protein binding competition and co-association tested by split-LUC assay in HeLa cells. HeLa cells experiments were performed in triplicates and repeated three times. Error bars indicate standard deviations. **e**, Co-immunoprecipitation of SHR, SCR and JKD from transfected *Nicotiana benthamiana* leaves. CoiP experiments for SCR, SHR and JKD were done seven times; experiments including negative controls were done two times. Full scan gels of one experiment can be found in the Supplementary Information.

Extended Data Figure 9 | Spatial network distribution specifying distinct cell types. Scheme representing the spatial protein complex distribution and the cellular sub-networks in the QC, CEI, meristemic endodermis and mature endodermis. SHR moves from the vasculature to the U-shaped domain where a close association with JKD in the QC leads to *WOX5* expression and QC specification, a close association to SCR in the CEI activates *CYCD6;1* and promote formative divisions, while its association to closely conjoint SCR and JKD leads to endodermal specification.

extended data table 1 | F r e t quantifications displayed as intensity based relative to: the positive control (upper rows), the maximal F r e t state (dA) (middle rows) and the estimated Förster resonance energy transfer (*E*) (lower rows)

Upper rows (light purple): Intensity-based FRET fraction relative to NLS:YFP:RFP. The relative intensity contribution of the FRET state was determined using triple lifetime unmixing of the phasors in the polar plot: the FRET phasor, the auto-fluorescence phasor (at ≈1.93 ns) and the control phasor (at ≈3.21 ns) in Fig. 1. For each transcription factor pair and cell type, the fractional intensity contribution of the FRET state relative to the control state was calculated and normalized to that of the average of the positive control NLS:YFP:RFP. By using this approach, the contribution of the auto-fluorescence component is removed from the FRET analysis. CI represents the 95% confidence interval and was calculated using statistical bootstrapping of the control and sample phasor clouds. Graphically, the calculation can be understood by extrapolating the line connecting the white filled diamond marker and the coloured filled circle marker in the polar plot and finding the intercept with the top dashed line of the triangular shape in the polar plot indicated in Fig. 1. The percentages in the table correspond to the distance between the filled triangle markers and this intercept point relative to that of the positive control.
Middle rows (light orange): intensity-based FRET fraction with respect to the maximal FRET state (DA). The lifetime of the FRET state was estimated to be around 1.93 ns, which corresponded to a maximum possible FRET value of $E\mathrm{max}=40\%$, this assuming an estimated donor life time of 3.21 ns. The relative intensity contribution of the FRET state was determined using triple lifetime unmixing of the phasors in the polar plot, thus removing the auto-fluorescence component from the FRET analysis. Graphically, the percentages in the table correspond to the distance between the filled triangle markers and the intercept point relative to the length of the top side of the triangular shape in Fig. 1.
Lower rows (light blue): estimated Förster resonance energy transfer (*E*), for the different transcription factor pair combinations and cell types. The *E*-value can be directly calculated using the formula $E=\alpha\mathrm{DA}\times E\mathrm{max}$.
When the confidence interval does not contain zero (black numbers), it is likely, or at 95% confidence that the estimated values are higher than zero and FRET occurs.